Elastic deformation as a tool to investigate watershed storage connectivity

Check for updates

Noah Clayton[1,5], Ellen Knappe[1,2], Alissa M. White[1,6], Hilary R. Martens[1], Donald F. Argus[3], Nicholas Lau[2], Adrian A. Borsa [2], Rebecca Bendick[1,4] & W. Payton Gardner [1] ✉

Storage-discharge relationships and dynamic changes in storage connectivity remain key unknowns in understanding and predicting watershed behavior. In this study, we use Global Positioning System measurements of load-induced Earth surface displacement as a proxy for total water storage change in four climatologically diverse mountain watersheds in the western United States. Comparing total water storage estimates with stream-connected storage derived from hydrograph analysis, we find that each of the investigated watersheds exhibits a characteristic seasonal pattern of connection and disconnection between total and stream-connected storage. We investigate how the degree and timing of watershed-scale connectivity is related to the timing of precipitation and seasonal changes in dominant hydrologic processes. Our results show that elastic deformation of the Earth due to water loading is a powerful new tool for elucidating dynamic storage connectivity and watershed discharge response across scales in space and time.

The relationship between water storage and stream discharge is a fundamental characteristic of watersheds and is required to properly forecast a watershed's response to climatic forcing. Watersheds are comprised of many different reservoirs, including surface water, snowpack, shallow soils, saprolite, bedrock, and vegetation, all of which experience temporally varying connections and disconnections to streams. However, measuring changes in total water storage in all reservoirs across the watershed presents many challenges. The ability to quantify the state of storage connection across the watershed, and determine the degree to which total storage is connected to the stream would mark a substantial contribution for hydrologists and water managers.

The classical watershed mass-balance equation reads: $P - ET - Q = \Delta S^*$, where P is precipitation, ET is evapotranspiration, Q is discharge, and ΔS^* represents changes in stream-connected storage. However, stream-connected storage, S^*, is not necessarily equivalent to the total storage in all reservoirs[1–5]. Connections between reservoirs and the adjacent stream network depend not only on the type of reservoir, but also on the reservoir storage conditions[2,3,6,7], and can be represented by a time-varying storage selection function[8–10]. Changing connections can lead to a non-linear response of watershed discharge to storage changes. Depending on the current state of storage, a given input of precipitation can produce different changes in discharge[11]. For example, snow falling during the winter adds to snowpack accumulation but does not concomitantly produce higher discharge. Advanced methods for characterizing the relationship between storage and discharge in complex terrain remain a fundamental pursuit in hydrologic studies[4,5,12–16].

Measurements of changes in total water storage over time could provide critical constraints on watershed behavior; however, monitoring storage in all terrestrial reservoirs across a watershed is challenging[5]. Point measurements of storage can be made accurately at high temporal resolution for individual reservoirs, such as vegetation[17], soil water[2,17,18], and bedrock groundwater[19,20]. However, point measurements are difficult to upscale due to strong spatial and temporal heterogeneities. Water balance methods suffer from large uncertainties in their inputs (e.g., precipitation) and outputs (e.g., evapotranspiration)[4,17,21–23].

The emerging field of hydrogeodesy presents new opportunities to estimate changes in total water storage at the watershed scale. The earth deforms elastically due to the total weight of water stored in all reservoirs at and near the surface of the earth. Elastic deformation of the Earth's surface due to water loading and unloading can provide information on fluctuations in total water storage at sub-seasonal temporal resolution[24–29]. Increases (decreases) in water storage manifest in the geodetic signal as a downward (upward) displacement of the Earth's surface[30–32]. Long records of precise Global Positioning System (GPS) inferred surface displacement can be

[1]Department of Geosciences, University of Montana, Missoula, MT, USA. [2]Institute of Geophysics and Planetary Physics, Scripps Institution for Oceanography, University of California San Diego, San Diego, CA, USA. [3]Jet Propulsion Laboratory, California Institute of Technology, Pasadena, CA, USA. [4]UNAVCO, Missoula, MT, USA. [5]Present address: Silixa, Missoula, MT, USA. [6]Present address: United States Geological Survey, Arizona Water Science Center, Yuma, AZ, USA. ✉e-mail: payton.gardner@umontana.edu

filtered and processed to isolate hydrologic responses and then inverted to estimate the total water storage[26,28]. However, total water storage inversion results are poorly constrained in areas of low GPS station density, which limits the use of GPS-inferred storage to basins with dense GPS arrays.

Estimated seasonal fluctuations in surface water mass over the central Amazon basin from a single GPS station show strong anticorrelation with the local stage height of the Amazon River[33], indicating that single station GPS observations can be informative of large watershed storage and discharge. For hydrological loading in the mountainous regions of western United States, GPS-observed vertical displacements are most strongly correlated with snow load within about 30 km of the station[34], consistent with surface-loading theory, which shows that the displacement response of the solid Earth to loading and unloading is largest at the center of the load and decays with distance[35,36], indicating that GPS station displacement is well correlated to loading at spatial scales on the order of tens of km. Thus, GPS observations of surface displacement from one or more stations could fill an important spatial gap between point-based measurements and regional-scale observations of water mass changes from satellites (e.g., the NASA-DLR GRACE mission) even in areas of poor GPS density.

In this paper, we explore the use of surface displacements measured by individual GPS to estimate total terrestrial hydrologic storage and storage connectivity at the intermediate watershed scale. We isolate the GPS Vertical Displacements (GPSVD) from hydrologic loading as an estimate of total water storage, which includes changes in storage for all hydrologic reservoirs regardless of their connection to the stream. We estimate the stream-connected storage, by quantifying the storage-discharge relationship for our watersheds and then inferring storage from observed discharge to give us the Discharge Inferred Storage (DIS). We then compare and contrast seasonal patterns of the GPSVD and the DIS, in four different watersheds across the western US (Fig. 1). We show that GPSVD can be used to quantify watershed connectivity, and that the relationship between GPSVD and DIS varies depending upon catchment climatology. We identify periods of the year when GPSVD is strongly correlated to DIS, and periods when the connection is not strong. Our results indicate that geodetic tools can provide

information on seasonal changes in the storage-discharge relationship and watershed sensitivity to precipitation. The results presented here are of interest for hydrologists and watershed managers looking to improve predictions of a watershed's unique response to climatic forcing, and to those looking to eventually operationalize geodetic information in hydrology, even in areas with limited GPS coverage.

Results

All studied watersheds exhibited seasonal patterns in precipitation, snow water equivalent (where applicable), discharge, and GPSVD[37] (Fig. 2). For the two snow-dominated watersheds (Camas Creek and Roaring Fork), the snow water equivalent starts building in November, peaks in March and April, respectively, and disappears by late May (Fig. 2a, b). Discharge peaks in April and June, respectively, as a result of snowmelt. In the Roaring Fork, discharge largely recesses from its peak until snowmelt begins again the following year. In Camas Creek, discharge recesses through late summer, and then increases to a higher fall or winter baseflow. In both watersheds, snow accumulation in the winter applies increasing pressure to the Earth's surface, which is observed as a downward displacement in the GPS record. Peak downward displacement occurs slightly after peak snow water equivalent when the total hydrologic load (i.e., snow, surface water, soil water, and groundwater) is at a maximum. According to the GPS, the surface subsequently rebounds for the rest of summer, with peak upward displacement in September when total water storage is at a minimum.

For the two rain-dominated catchments (West Fork (W. Fk.) of the Russian and North Yuba), precipitation occurs primarily during the fall and winter (October–May) and is followed by a dry period during the summer (June–September) (Fig. 2c, d). In both watersheds, discharge increases sharply in the fall with the onset of precipitation. In the W. Fk. Russian, discharge rates level off in December but remain high for the rest of the winter. In the North Yuba, discharge rates continue to increase until dry summer conditions return. GPSVD for these rain-dominated watersheds shows a peak downward displacement in April and a peak upward displacement in August to September.
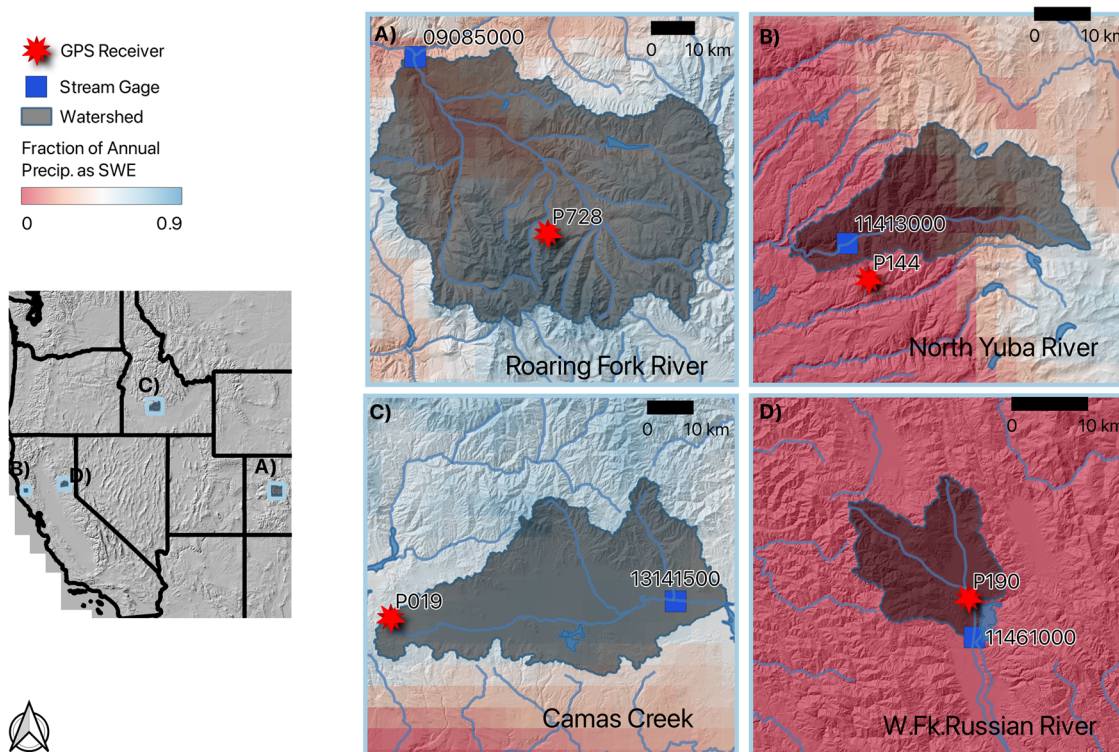

Fig. 1 | Map of study watersheds. Map of study watersheds in the western US showing GPS stations as red stars and USGS stream gauge locations as blue squares. Inset maps (**A**–**D**) are colored by the ratio of the average April 1 snow water equivalent to the total average annual precipitation[47].
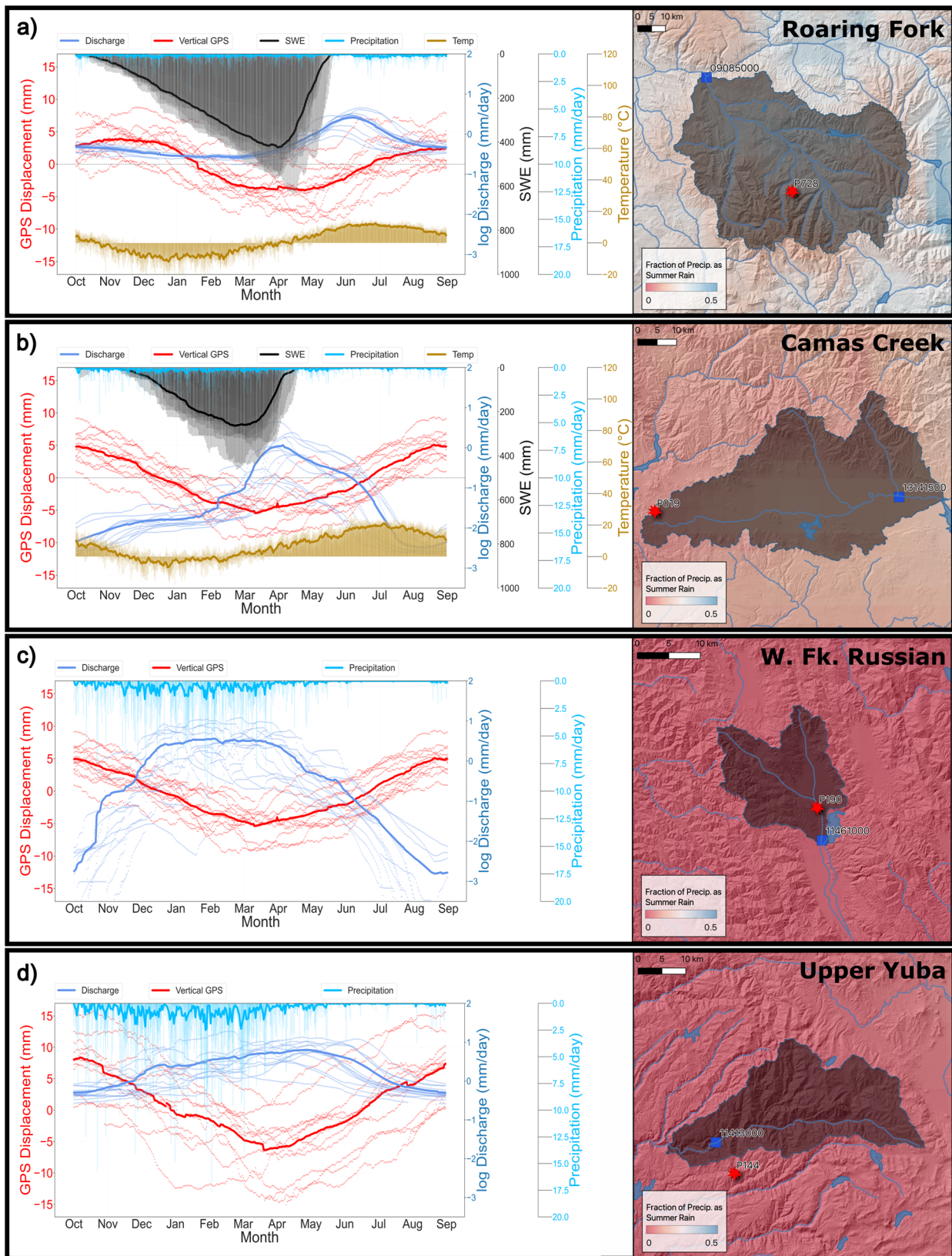
Fig. 2 | Hydrologic and GPS annual trends. Time series of precipitation (light blue), discharge (dark blue), snow water equivalent (black), temperature (gold), and GPS vertical displacement (GPSVD) (light red) for each of the four watersheds (**a–d**). Global position system stations are located within, or proximal to the watersheds. Annual signals for all years of combined record (the faint lines in the background) and mean for all years (bold lines) are shown (**a–d**). The fraction of average annual precipitation falling in the summer months is shown on maps on the right side of each panel[47].
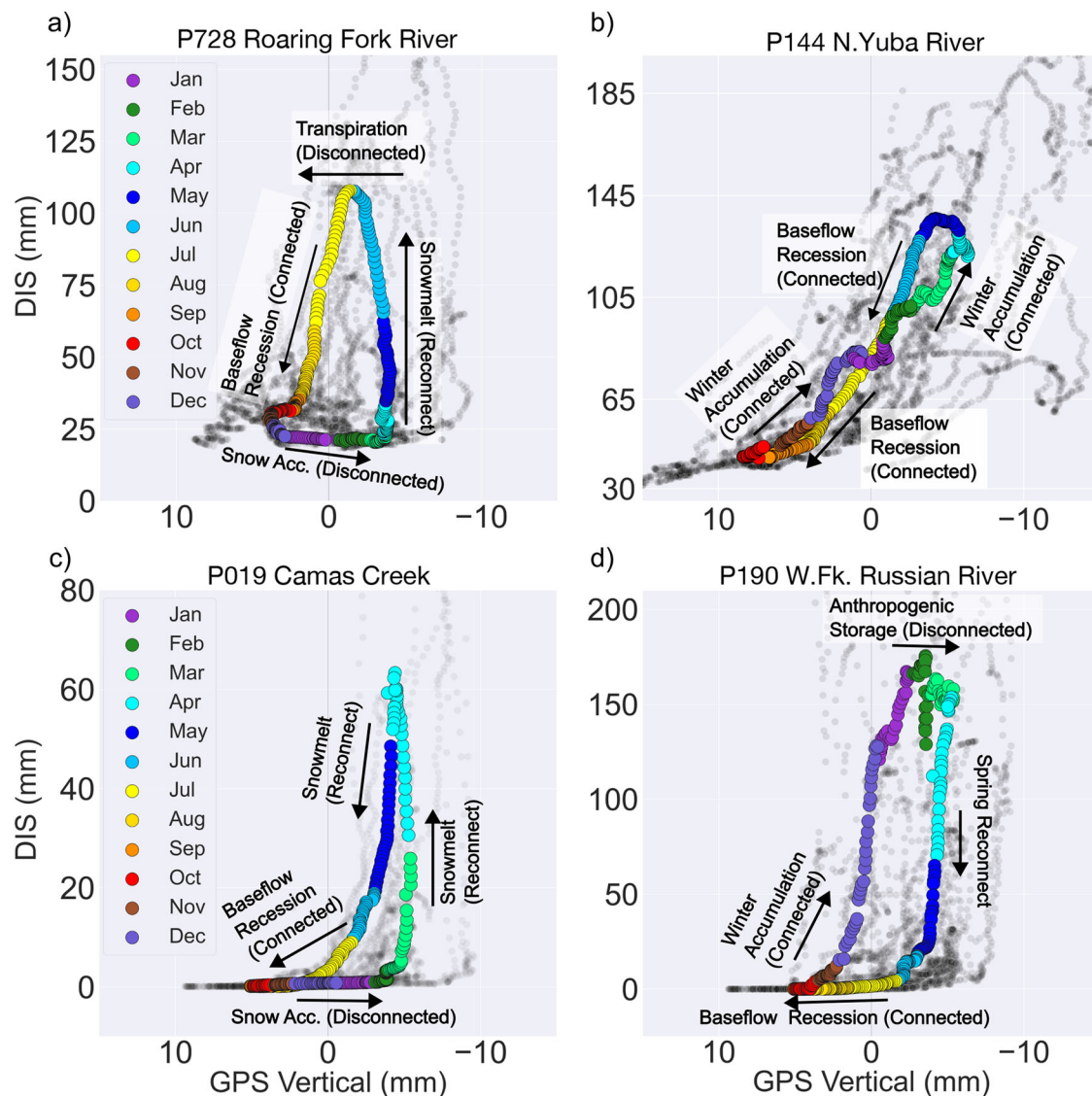
Fig. 3 | Storage hysteresis plots. Discharge inferred storage (DIS) vs. GPS vertical displacement (GPSVD) plots for **a** Roaring Fork, **b** North Yuba, **c** Camas Creek, and **d** W. Fk. of the Russian River watersheds. Individual days for all years on record are plotted in light gray, and the median values for the period of record are plotted as opaque symbols, colored by month. Arrows indicate the direction of the loop, major times of connection and disconnection and potential processes affecting the watershed during these times. All discharge-inferred storage and GPSVD time series are smoothed with a 30 day average filter. Note that the *x*-axis is flipped so that slope values are positive when storage and streamflow are connected.

Figure 3 shows the changes in discharge-inferred storage (DIS) relative to GPSVD. We averaged 11 years of observations to derive a characteristic annual DIS-GPSVD curve for each watershed, whose hysteresis (i.e., seasonal pattern of response lag between total and stream-connected storage) provides information on the average of storage partitioning for each watershed.

GPSVD and DIS in the four watersheds fluctuate seasonally. For example, in the snow-dominated Roaring Fork River watershed, GPSVD steadily increases with snow accumulation from October–February (Fig. 3a), while DIS remains flat or slightly decreases as water remains locked in the snowpack. During the spring months of March–June (Fig. 3a), DIS rapidly increases alongside uplift in the GPSVD, implying that an increasing fraction of storage becomes stream-connected during this period. During the summer months (July–September; Fig. 3a), diminishing DIS is coupled with a loss of total storage. Camas Creek, the other snow-dominated watershed, shows a similar strong snowpack accumulation period from October–February, during which DIS remains

relatively constant, followed by rapid reconnection in March or April and a long recession period from May–September (Fig. 3c).

In contrast, in the rain-dominated North Yuba River watershed, DIS and GPSVD covary linearly and show only subtle hysteresis behavior throughout the year (Fig. 3b). The West Fork Russian River behaves similarly to North Yuba early in the winter, when a relatively rapid increase in DIS is accompanied by downward movement of the GPSVD (Fig. 3d). However, DIS levels off in late winter, even as GPSVD continues to trend downward.

To explore patterns in storage connectivity, we define periods of high connectivity as times when the DIS and GPSVD vary together, with inferred storage changes in the same direction (i.e., a negative slope of DIS vs GPSVD ($m < -0.25$) and strong correlation ($R^2 > 0.7$)). A negative slope indicates a decrease in stream-connected storage when the GPSVD exhibits upward displacement (a decrease in total storage). We evaluated the linear regression over a 45-day window of the 11-year average GPSVD and DIS to quantify seasonal patterns in slope and covariance between GPSVD and DIS.
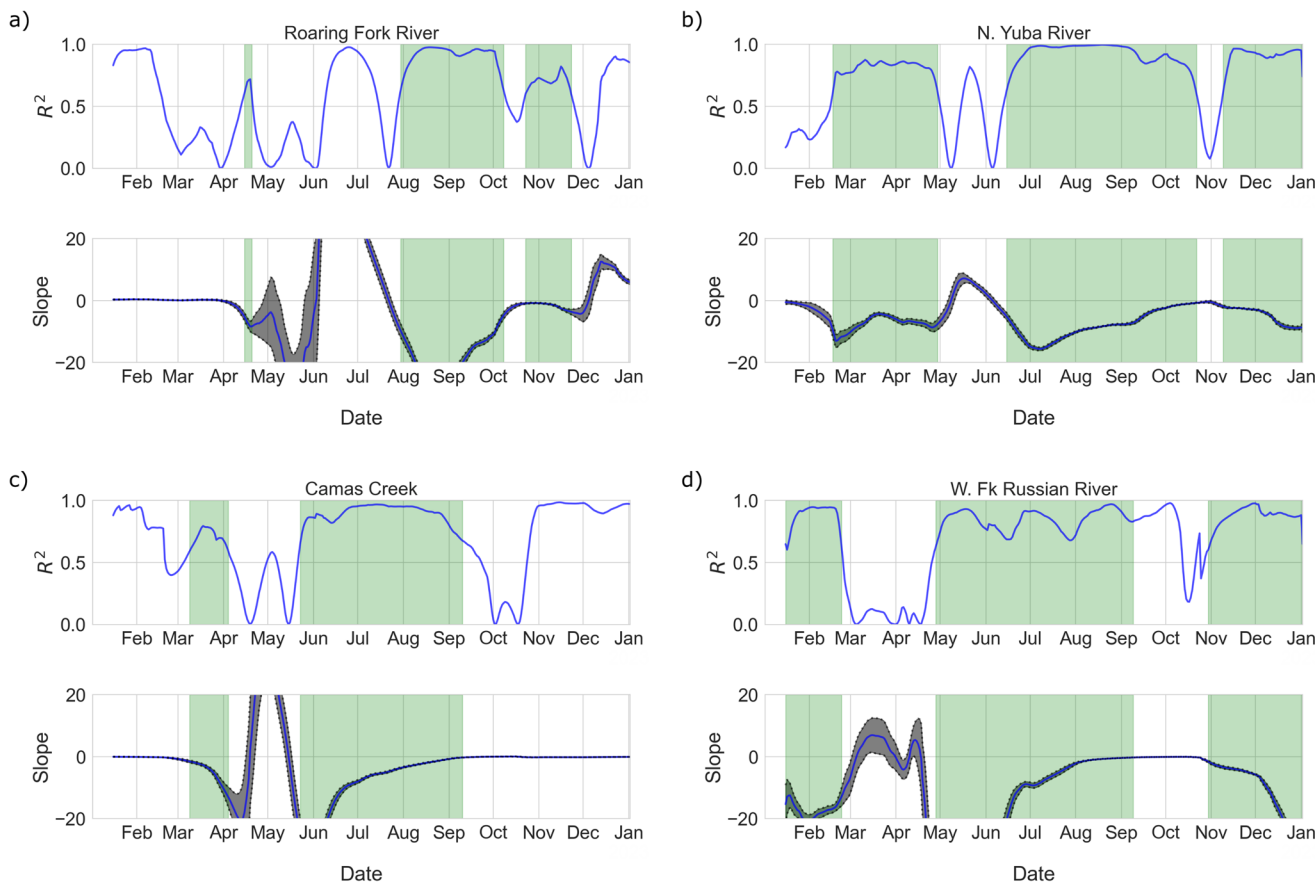
Fig. 4 | Watershed connectivity. Rolling correlation coefficient (top panel of each pair) and ordinary least-squares linear slope estimate (bottom panel of each pair), for **a** Roaring Fork, **b** North Yuba, **c** Camas Creek, and **d** W. Fk. of the Russian River watersheds. Rolling coefficients were calculated for a 45 day window. The slope estimates include 5th and 95th percentile confidence intervals assuming a normal distribution of error variance. Green shaded areas mark highly connected periods, where GPSVD and discharge-inferred storage have a slope of -0.25, and an $R^2 > 0.7$. A negative GPS displacement indicates increased storage.

Our correlation analysis highlights periods that exhibit stream-connected (green) and stream-disconnected (white) storage behaviors (Fig. 4). Each watershed exhibits a unique pattern of connection in terms of timing and duration. In general, rain-dominated watersheds experience higher stream connectivity for a majority of the year. We find that the rain-dominated North Yuba River is connected for the longest duration, with a total of 257 days of high connectivity across all seasons. For example, a period of almost continuous connection occurs in the North Yuba between June and January, with a break in October and November, and is again highly connected in March through May. The rain-dominated W. Fk. Russian River is highly connected for ~239 days, with a long period of connection from May through September and again from November through March.

Overall, the two snow-dominated watersheds exhibited weaker connectivity. Camas Creek is highly connected for 138 days of the year, with a long period of connection occurring from June through September and a short period in March and April. The Roaring Fork shows the lowest connection, with only 109 days of high connectivity, mostly between August and December.

Discussion

Annual patterns of stream connection and disconnection to storage led to different relationships between GPSVD (total) and DIS (stream-connected) in the four study watersheds. The partitioning of storage between stream-connected and stream-disconnected reservoirs is expected to be a complex function of topography, ecology, climate, and geology, and our results show that GPSVD can provide insight into how these factors operate in the context of individual watersheds.

Watersheds exhibit distinct periods of enhanced connection between storage and discharge, whereby changes in total water storage are strongly and positively correlated with discharge. During these periods, an increase (decrease) in total storage results in a nearly simultaneous (i.e., little to no phase lag or lead) increase (decrease) in stream-connected storage. GPSVD is a strong predictor of discharge during these periods.

Conversely, our results also reveal distinct periods when total water storage and stream-connected storage are disconnected. During these periods, a change in GPSVD can be uncorrelated or even anti-correlated to a change in DIS. The disconnection of total storage and discharge-inferred storage is consistent with a variety of processes in the watershed. The disconnection could be due to stream discharge and ET coming from separate, unconnected reservoirs; water stored in static snowpacks[38–40]; or water stored in unsaturated, unconnected soil reservoirs. GPSVD displacement provides minimal information on stream discharge during these periods. The hysteresis loops shown in Fig. 3 are consistent with those generated for snow-dominated watersheds using data from the GRACE satellite mission[41] and provide important information on watershed-scale processes and behaviors. Our results suggest that GPSVD, even from a single station, can provide useful information for hydrologists.

In all watersheds investigated here, a strong connection is observed during the dry-season recession period in the summer and fall. For the seasonally dry North Yuba River, W. Fk. Russian River, and Camas Creek watersheds, the connected period begins in mid to late June and lasts into September. For the summer monsoonal Roaring Fork watershed, the dry period begins in mid-August and lasts through October. We interpret the dry period as one where snowmelt (and monsoonal precipitation) is largely finished for the season, available soil water is mostly depleted (so actual ET is

reduced), and groundwater discharge to streams (baseflow) represents the dominant form of storage change in the watershed. The beginning and ending of these periods are consistent with the climatology of the watersheds, where seasonally dry watersheds receive little precipitation through July and August, and, in contrast, summer monsoon watersheds receive appreciable rainfall during July and August. For snow-dominated watersheds, a clear snow accumulation signal can be seen from October through March. Snowpack dominates changes in total water storage during this period, and the snowpack (prior to melting) remains disconnected from stream discharge.

Sudden episodes of reconnection follow disconnected states and are marked by a rapid increase in discharge at relatively constant total storage. The sudden reconnection indicates that storage in the watershed can transition rapidly to reservoirs with strong stream connections. The shape and slope of the reconnection period in the storage-discharge diagram (Fig. 3) provide insight into watershed dynamics, including the transfer of water between stream-disconnected and connected reservoirs over the year.

During snowmelt in April–May in the Camas Creek watershed, discharge rapidly increases, while inferred total storage stays constant, suggesting that melting snowpack infiltrates the soils and undergoes lateral subsurface flow. Conversely, the reconnection period in the Roaring Fork watershed shows an anticorrelated relationship in which total storage decreases even as discharge inferred storage increases. This anticorrelation is consistent with an increased transfer of water to stream-connected reservoirs, even as total storage drops, indicating additional loss of storage to a non-stream-connected reservoir such as the atmosphere. The additional loss could be explained by loss of snowmelt to evapotranspiration and sublimation, rather than to stream-connected reservoirs.

The rain-dominated Russian River exhibits disconnection during late winter and early spring, wherein discharge remains relatively constant while storage continues to increase. This signal could be the result of artificial reservoir operations at Lake Mendocino on the nearby East Fork Russian River or at Clear Lake on the Cache Creek drainage. Neither of the reservoirs would have a large effect on the West Fork discharge but would appreciably influence the GPS-inferred ground displacement. Artificial storage management can affect either the actual storage discharge relationship in a given watershed, or affect GPSVD by signal leakage to nearby watersheds.

The estimate of the connection between total storage and stream discharge depends on the thresholds assumed here for slope (-0.25) and correlation (0.7). Here, we require a negative slope with a steepness >0.25 to classify a stream as highly connected to the total storage. This slope was chosen as a conservative boundary, where the 95% uncertainty bounds of the estimate slope remained below zero (Fig. 4). Furthermore, we adopt a minimum R^2 threshold of 0.7 to ensure that the association between storage and discharge is reasonably strong. These cutoffs are somewhat arbitrary, but are conservative indications of strong connection, and allow for quantitative intercomparison of the watersheds. Experimentation with both cutoffs revealed slightly different numbers of high-connection days during the year; however, the general connectivity patterns remained consistent, largely due to the sharp gradients in both metrics during disconnection and reconnection (Fig. 4).

GPS displacements are most sensitive to nearby loading, yet they also contain information about "far-field" loading external to the watershed[34–36]. Our data processing removes the atmospheric loading component and the common mode to reduce regional signal, yet these single datasets still contain some signal from far-field regional hydrologic loading. If regional loading was dominant, we would expect all stations to covary. Overall, we find that the correlation between individual GPS stations ranges between 0.5 and 0.7, indicating that regional covariance is moderate to strong but that inter-station differences do exist.

We also test for the effects of regional loading using GPS-inferred storage from all GPS stations. The inversion of GPS displacement data for water-mass distribution from a dense and widespread network of GPS stations, combined with far-field load removal and reference frame jitter

correction, mitigates the influence of far-field loads on the storage-discharge curve[26,28]. Stream discharge could be compared directly with GPS-constrained estimates of total-storage changes within the watershed rather than with GPS displacements, which contain information about both local- and regional-scale loads. We compared inverted water storage changes across our watersheds with DIS in an analysis, like that done for GPSVD. We observed similar results for the California watersheds, but little pattern for the Colorado and Idaho watersheds. Uncertainties in GPS inversions depend strongly on the number of stations available and become highly uncertain in areas with poor coverage[42]. California has relatively dense arrays of GPS stations due to active monitoring of the tectonic-plate boundaries along the US west coast; however, the Rocky Mountains (as well as smaller individual watersheds in California) have only sparse instrumentation.

We compared GPSVD, DIS, and monthly estimates of total water storage estimated using the geodetic inversion methods of Argus et al. (2017). The GPS-inverted storage and GPSVD are moderately to well correlated in California ($R^2 = 0.5$), but show poor correlation ($R^2 = 0.07$) for the northern and southern Rocky Mountains, where GPS networks are sparse (Supplementary Methods). These results indicate that GPSVD generally reflects inverted storage in the watersheds where station coverage is high. We further explore the ability of GPSVD to measure local watershed loading by measuring the correlation between inverted storage and GPSVD with the independent DIS storage measure. During periods of expected high stream connectivity, GPSVD shows a stronger correlation to DIS ($\bar{R}^2 = 0.5$) than GPS-inverted storage ($\bar{R}^2 = 0.3$) (Supplementary Methods), indicating GPSVD is doing as well or perhaps better at capturing local watershed storage changes.

The similar correlation between GPSVD and inferred storage from geodetic inversion in areas with dense GPS coverage (where we expect the highest accuracy of inversion), along with the strong correlation of GPSVD and DIS during highly connected periods, supports the hypothesis that single-station GPS displacements can characterize the state of total storage in relatively small watersheds (100–1000 km² HUC 8–10). As geodetic data and models improve coverage and accuracy, we suggest that inversion products be used in place of GPS displacements. While we cannot completely remove the effect of regional loading, it appears GPSVD, even at a single station, can provide valuable insights to hydrologists on storage-discharge relationships at high temporal resolution, even in areas with limited GPS coverage. The relationships between storage and discharge, informed by GPS geodesy, can be used to better understand watershed processes and behavior and eventually to improve forecasts of watershed response. By introducing these geodetic methods to the hydrologic community, we anticipate spawning future improvements in both hydrologic and GPS analysis and interpretation.

Materials and methods

We report results from four western US watersheds: two snow-dominated and two rain-dominated of intermediate scale (~100–3000 km²) (Fig. 1). These watersheds were chosen to explore a range of precipitation amounts, types, and timing as well as to include at least 10 years of GPS and discharge data. Each watershed has a NOTA (Network of the Americas) GPS station within or near (within ~10 km) the watershed boundary as well as an existing USGS streamflow gauge with a minimum of 10 years of concurrent discharge data.

The two snow-dominant watersheds are the seasonally dry Camas Creek (1621 km², $E_{avg} = 1710(1456 - 3061)masl$), located in the Northern Rockies of Idaho, and the summer-monsoonal watershed of the Roaring Fork River watershed (3763 km², $E_{avg} = 2931(1759 - 4247)masl$), located in the central Rocky Mountains of western Colorado. Both snow-dominated watersheds have long, cold winters marked by snowpack accumulation from November through April (Fig. 1 and Fig. 2). In the seasonally dry Camas Creek, precipitation is low during July, August, and September (Fig. 2). In the Roaring Fork Watershed, summer monsoon rains begin in early July and last through August (Fig. 2).

The two rain-dominant watersheds are the West Fork of the Russian River (259 km^2, $E_{avg} = 450(189 - 1019)masl$) and the North Yuba River (648 km^2, $E_{avg} = 1673(674 - 2525)masl$), both located in California. These watersheds have temperate Mediterranean climates, with cool and wet winters (November–June), followed by hot and dry summers (July–September). The North Yuba is located in the moderate elevation northern Sierra Nevada Mountains. The upper portions of the watershed receive short-lived snow in the winter; however, we consider the North Yuba to be a rain-dominated watershed in this study.

We define "total water storage" as the volume of water stored in all terrestrial reservoirs, regardless of their direct connection to the stream network. A "direct connection" implies that changes in one reservoir have a near-in-time (within a few days) effect on another watershed component. We define "stream-connected storage reservoirs" as those having a direct impact on stream discharge at a given time.

The stream-connected or dynamic storage[5] can be inferred from the measured stream discharge, Q, by estimating the storage-discharge relationship during periods of low P and ET (cf. Kirchner, 2009; see Supplemental Material for details). For each watershed in our analysis, we parameterized discharge-inferred storage by fitting a power-law discharge relationship during periods of low ET and P[15]:

$$\frac{dQ}{dt} = -\alpha Q^\beta \qquad (1)$$

where α and β are the power law coefficients estimated for each basin from the best-fit discharge relationship. These parameters were then used to infer the change in storage (ΔS^*) via:

$$\Delta S^* = \frac{1}{\alpha}\frac{1}{(2-\beta)}Q^{(2-\beta)} \qquad (2)$$

Instantaneous stream discharge (cfs) was obtained from the USGS (waterwatch.usgs.gov), averaged over each day to calculate a mean daily discharge, normalized by the watershed area above the gauge, and converted to mm/d.

We used GPS vertical displacement (GPSVD) as a proxy for changes in total water storage[26,28,30,35]. To isolate the hydrological loading signal within the GPS data, we began with a time series of daily position estimates from UNAVCO's Central Washington University processing center in the IGS14 reference frame[43] (https://www.unavco.org/data/data.html). Solid-body tides and oceanic load tides were removed during initial processing. We then removed contributions to the vertical displacement time series from non-tidal atmospheric pressure loading and non-tidal oceanic loading using ESMGFZ products[44]. Discrete offsets in the time series were removed based on the UNAVCO catalog using a Heaviside function, which can be found in the Supplementary Methods[45]. Outliers were removed from the series using a moving 90 day median absolute deviation filter; any GPS positions that fell outside three absolute deviations of the median were discarded[46]. A best-fit linear trend was then subtracted from each time series to remove long-term tectonic signals. Common mode components in GPS data, network-wide, spatially correlated signals due to global loading, systematic processing errors, or uncertainties (e.g., reference frame realizations, tropospheric mapping functions, clocks, and orbits) were removed using a seven-parameter Helmert transformation. After using GRACE as a first-order transient deformation correction, both vertical and horizontal data from all stations within the network were used to estimate the best-fit Helmert transformation parameters.

For both GPSVD and stream discharge, we smoothed the time series using a 30 day moving average. The average values of displacement and discharge were then calculated for each calendar day over the period of record (daily average). The record lengths of the GPS time series limited the study period; for the continuous GPS stations considered here, we had at least 11 years of data at each site. We converted standard calendar days to days of the water year (i.e., Oct 1 = Day 1 and Sept 30 = Day 365; leap-year days (366) were omitted).

Data availability

Code availability

References

1. Enzminger, T. L., Small, E. E. & Borsa, A. A. Subsurface water dominates sierra nevada seasonal hydrologic storage. *Geophys. Res. Lett.* **46**, 11993–12001 (2019).
2. Jencso, K. G. et al. Hydrologic connectivity between landscapes and streams: transferring reach- and plot-scale understanding to the catchment scale. *Water Resour. Res.* **45**, W04428 (2009).
3. Jencso, K. G., McGlynn, B. L., Gooseff, M. N., Bencala, K. E. & Wondzell, S. M. Hillslope hydrologic connectivity controls riparian groundwater turnover: implications of catchment structure for riparian buffering and stream water sources. *Water Resour. Res.* **46**, W10524 (2010).
4. Kuppel, S., Tetzlaff, D., Maneta, M. P. & Soulsby, C. Critical zone storage controls on the water ages of ecohydrological outputs. *Geophys. Res. Lett.* https://doi.org/10.1029/2020GL088897 (2020).
5. Staudinger, M. et al. Catchment water storage variation with elevation. *Hydrol. Process.* **31**, 2000–2015 (2017).
6. Grayson, R. B., Western, A. W., Chiew, F. H. S. & Blöschl, G. Preferred states in spatial soil moisture patterns: local and nonlocal controls. *Water Resour. Res.* **33**, 2897–2908 (1997).
7. Western, A. W., Grayson, R. B., Blöschl, G., Willgoose, G. R. & McMahon, T. A. Observed spatial organization of soil moisture and its relation to terrain indices. *Water Resour. Res.* **35**, 797–810 (1999).
8. Benettin, P., Van Der Velde, Y., Van Der Zee, S. E. A. T. M., Rinaldo, A. & Botter, G. Chloride circulation in a lowland catchment and the formulation of transport by travel time distributions. *Water Resour. Res.* **49**, 4619–4632 (2013).
9. Harman, C. J. Time-variable transit time distributions and transport: theory and application to storage-dependent transport of chloride in a watershed. *Water Resour. Res.* **51**, 1–30 (2015).
10. Rinaldo, A. et al. Storage selection functions: a coherent framework for quantifying how catchments store and release water and solutes. *Water Resour. Res.* **51**, 4840–4847 (2015).
11. Berghuijs, W. R., Hartmann, A. & Woods, R. A. Streamflow sensitivity to water storage changes across Europe. *Geophys. Res. Lett.* **43**, 1980–1987 (2016).
12. Berghuijs, W. R. & Kirchner, J. W. The relationship between contrasting ages of groundwater and streamflow. *Geophys. Res. Lett.* **44**, 8925–8935 (2017).

13. Bergstrom, A., Jencso, K. & McGlynn, B. Spatiotemporal processes that contribute to hydrologic exchange between hillslopes, valley bottoms and streams. *Water Resour. Res.* **52**, 4628–4645 (2016).

14. Brooks, P. D. et al. Hydrological partitioning in the critical zone: recent advances and opportunities for developing transferable understanding of water cycle dynamics. *Water Resour. Res.* **51**, 6973–6987 (2015).

15. Kirchner, J. W. Catchments as simple dynamical systems: catchment characterization, rainfall-runoff modeling and doing hydrology backward. *Water Resour. Res.* **45**, W02429 (2009).

16. Maxwell, R. M. et al. The imprint of climate and geology on the residence times of groundwater. *Geophys. Res. Lett.* **43**, 701–708 (2016).

17. Hoylman, Z. H. et al. The climatic water balance and topography control spatial patterns of atmospheric demand, soil moisture and shallow subsurface flow. *Water Resour. Res.* **55**, 2370–2389 (2019).

18. Jencso, K. G. & McGlynn, B. L. Hierarchical controls on runoff generation: topographically driven hydrologic connectivity, geology and vegetation. *Water Resour. Res.* https://doi.org/10.1029/2011WR010666, W11527 (2011).

19. Gabrielli, C. P., Morgenstern, U., Stewart, M. K. & McDonnell, J. J. Contrasting groundwater and streamflow ages at the maimai ewatershed. *Water Resour. Res.* **54**, 3937–3957 (2018).

20. Hale, V. C. et al. Effect of bedrock permeability on stream base flow mean transit time scaling relationships: 2 process study of storage and release. *Water Resour. Res.* **52**, 1375–1397 (2016).

21. Daly, C. et al. Physiographically sensitive mapping of climatological temperature and precipitation across the conterminous United States. *Int. J. Climatol.* **28**, 2031–2064 (2008).

22. Silverman, N. L., Maneta, M. P., Chen, S. H. & Harper, J. T. Dynamically downscaled winter precipitation over complex terrain of the central Rockies of Western Montana, USA. *Water Resour. Res.* **49**, 458–470 (2013).

23. Silverman, N. L. & Maneta, M. P. Detectability of change in winter precipitation within mountain landscapes: spatial patterns and uncertainty. *Water Resour. Res.* **52**, 4301–4320 (2016).

24. Adusumilli, S., Borsa, A. A., Fish, M. A., McMillan, H. K. & Silverii, F. A decade of water storage changes across the contiguous United States from GPS and satellite gravity. *Geophys. Res. Lett.* **46**, 13006–13015 (2019).

25. Argus, D. F., Fu, Y. & Landerer, F. W. Seasonal variation in total water storage in California inferred from GPS observations of vertical land motion. *Geophys. Res. Lett.* **41**, 1971–1980 (2014).

26. Argus, D. F. et al. Sustained water loss in California's mountain ranges during severe drought from 2012 to 2015 inferred from GPS. *J. Geophys. Res. Solid Earth.* **122**, 10,559–10,585 (2017).

27. Birhanu, Y. & Bendick, R. Monsoonal loading in Ethiopia and Eritrea from vertical GPS displacement time series. *J Geophys. Res. Solid Earth.* **120**, 7231–7238 (2015).

28. Borsa, A. A., Agnew, D. C. & Cayan, D. R. Ongoing drought-induced uplift in the western United States. *Science.* **345**, 1587–1590 (2014).

29. Fu, Y., Argus, D. F. & Landerer, F. W. GPS as an independent measurement to estimate terrestrial water storage variations in Washington and Oregon. *J. Geophys. Res. Solid Earth* **120**, 552–566 (2015).

30. Van Dam, T. et al. Crustal displacements due to continental water loading. *Geophys. Res. Lett.* **28**, 651–654 (2001).

31. Dong, D., Fang, P., Bock, Y., Cheng, M. K. & Miyazaki, S. Anatomy of apparent seasonal variations from GPS-derived site position time series. *J. Geophys. Res. Solid Earth* **107**, ETG 9-1–ETG 9-16 (2002).

32. Heki, K. Seasonal modulation of interseismic strain buildup in northeastern Japan driven by snow loads. *Science.* **293**, 89–92 (2001).

33. Bevis, M. et al. Seasonal fluctuations in the mass of the Amazon River system and Earth's elastic response. *Geophys. Res. Lett.* **32**, 1–4 (2005).

34. Knappe, E., Bendick, R., Martens, H. R., Argus, D. F. & Gardner, W. P. Downscaling vertical GPS observations to derive watershed-scale hydrologic loading in the northern rockies. *Water Resour. Res.* **55**, 391–401 (2019).

35. Farrell, W. E. Deformation of the Earth by surface loads. *Rev. Geophys.* **10**, 761–797 (1972).

36. Martens, H. R., Rivera, L., Simons, M. & Ito, T. The sensitivity of surface mass loading displacement response to perturbations in the elastic structure of the crust and mantle. *J. Geophys. Res. Solid Earth* **121**, 3911–3938 (2016).

37. Gardner, W. P. Data: Elastic deformation as a tool to investigate watershed storage connectivity [Data set]. In Nature Communications Earth and Environmental Sciences (Version 1). Zenodo. https://doi.org/10.5281/zenodo.7310090 (2023).

38. Evaristo, J., Jasechko, S. & McDonnell, J. J. Global separation of plant transpiration from groundwater and streamflow. *Nature.* **525**, 91–94 (2015).

39. McDonnell, J. J. The two water worlds hypothesis: ecohydrological separation of water between streams and trees. *Wiley Interdiscip. Rev. Water* **1**, 323–329 (2014).

40. Renée Brooks, J., Barnard, H. R., Coulombe, R. & McDonnell, J. J. Ecohydrologic separation of water between trees and streams in a mediterranean climate. *Nat. Geosci.* **3**, 100–104 (2010).

41. Sproles, E. A. et al. GRACE storage-runoff hystereses reveal the dynamics of regional watersheds. *Hydrol. Earth Syst. Sci.* **19**, 3253–3272 (2015).

42. Argus, D. F. et al. Subsurface water flux in California's Central Valley and its source watershed from space geodesy. *Geophys. Res. Lett.* **49**, e2022GL099583 (2022).

43. Blewitt, G., Hammond, W. & Kreemer, C. Harnessing the GPS data explosion for interdisciplinary science. *EOS (Washington DC).* **99**, https://doi.org/10.1029/2018EO104623 (2018).

44. Dill, R. & Dobslaw, H. Numerical simulations of global-scale high-resolution hydrological crustal deformations. *J. Geophys. Res. Solid Earth* **118**, 5008–5017 (2013).

45. Herring, T. A. et al. Plate boundary observatory and related networks: GPS data analysis methods and geodetic products. *Rev. Geophys.* **54**, 759–808 (2016).

46. Klos, A., Bogusz, J., Figurski, M. & Kosek, W. On the handling of outliers in the GNSS time series by means of the noise and probability analysis. *IAG. Symposia.* **0**, 657–664 (2016).

47. Luce, C. H., Lopez-Burgos, V. & Holden, Z. Sensitivity of snowpack storage to precipitation and temperature using spatial and temporal analog models. *Water Resour Res.* **50**, 9447–9462 (2014).

Acknowledgements

Author contributions

N.C.—data analysis, interpretation, writing, conception; E.K.—data analysis, interpretation, writing, conception; A.W.—data analysis, interpretation; H.M.—conception, data interpretation, project management; D.A.—data analysis, data interpretation, conception; N.L.—data analysis, interpretation, writing; A.B.—conception, data interpretation, project management, writing; R.B.—conception, project management, data

collection; P.G.—project management, conception, data analysis, interpretation, writing.

Competing interests

The authors state no competing interests.

Additional information